Albers *et al. Geothermal Energy* (2025) 13:34
https://doi.org/10.1186/s40517-025-00359-0

Geothermal Energy

RESEARCH Open Access

Depth-specific thermal conductivities of Triassic sandstones

Anna Albers[1*], Fabien Glatting[1], Kathrin Menberg[1], Hagen Steger[1], Christina Fliegauf[1], Linda Schindler[2], Sascha Wilke[1], Roman Zorn[2] and Philipp Blum[1]

*Correspondence:
anna.albers@kit.edu

[1] Karlsruhe Institute of Technology (KIT), Institute of Applied Geosciences (AGW), Kaiserstraße 12, 76131 Karlsruhe, Germany
[2] European Institute for Energy Research (EIFER), Emmy-Noether-Straße 11, 76131 Karlsruhe, Germany

Abstract

Triassic sandstones of the Middle and Upper Buntsandstein are highly suitable for ground source heat pump (GSHP) systems. Thus, knowledge of their thermal properties, which can be measured or estimated by theoretical models, is crucial. However, the transferability of estimated thermal conductivities to the field scale has not yet been thoroughly examined. Therefore, in this study, the thermal and lithological properties of 156 core samples from a borehole in the Buntsandstein are analysed in the laboratory. Various theoretical models are applied and compared to the laboratory-derived thermal conductivities. The best agreement is achieved with the Voigt-Reuss-Hill model with an average thermal conductivity of 4.5 W m^{-1} K^{-1} and an RMSE of 0.7 W m^{-1} K^{-1} (T = 20 °C). The results of this model are compared to depth-specific, effective thermal conductivities from an enhanced thermal response test (ETRT). These effective thermal conductivities range between 2.3 and 6.1 W m^{-1} K^{-1} with an average of 4.7 W m^{-1} K^{-1}. We demonstrate that some theoretical models can provide an initial estimation of the effective thermal conductivity of sandstones when groundwater flow is negligible. However, the accuracy of the estimation is limited by sample quantity and model assumptions.

Keywords: Enhanced thermal response test (ETRT), Porosity, Sandstone, Thermal conductivity models

Introduction

Carbon dioxide emissions from heating-related energy consumption can be reduced significantly by using shallow geothermal energy (Blum et al. 2010). Ground source heat pump (GSHP) systems using borehole heat exchangers (BHE) are the most popular shallow geothermal installations (Acuña and Palm 2010; Bayer et al. 2012). To size GSHP systems efficiently and ensure sustainable long-term operation, knowledge of the subsurface thermal properties at the system's site is crucial, with the thermal conductivity of the ground being the critical design property (Spitler and Gehlin 2015).

The Buntsandstein in the Central European Basin represents a significant geological formation from the early Triassic (Soyk 2015). Due to its typically high thermal conductivity (Franz and Schulze 2016; Haffen et al. 2017; Kämmlein and Stollhofen 2019a), the Buntsandstein is a favourable host rock for shallow geothermal applications.

Buntsandstein rocks were formed through diverse sedimentary environments and diagenetic processes, resulting in heterogeneous properties (Soyk 2015). Reported thermal conductivity of saturated laboratory samples varied significantly between 1.7 and 5.8 W m^{-1} K^{-1} at room temperature (Franz and Schulze 2016; Haffen et al. 2017; Kämmlein and Stollhofen 2019a).

The standard method for determining thermal conductivity in the context of GSHP systems is the thermal response test (TRT) (Spitler and Gehlin 2015), which produces estimates of effective thermal conductivities (λ_{eff}) of the subsurface at in-situ conditions. Further enhancements of the TRT were achieved by using fibre optic cables, which enable the determination of depth-specific effective thermal conductivity (Wilke et al. 2020). The so-called distributed thermal response tests (DTRT) use distributed temperature sensing (DTS) in combination with a circulating heat transfer fluid, whereas enhanced thermal response tests (ETRT) combine DTS with a heating cable (Wilke et al. 2020).

The main disadvantage of in-situ TRTs is that they are expensive and time-consuming (Abuel-Naga et al. 2009). A cost-effective alternative is to measure thermal conductivity in the laboratory. The transient half-space probe line source method (e.g. Jorand et al. 2015; Kämmlein and Stollhofen 2019a) and the optical scanning method (e.g. Franz and Schulze 2016; Popov et al. 1999) are commonly applied to measure the thermal conductivity of sandstones. Yet, only a few studies (e.g. Ma et al. 2022) compare ETRT results with high-resolution borehole data from laboratory measurements.

As an alternative to in-situ TRTs or laboratory measurements, various theoretical models were suggested to estimate the thermal conductivities based on petrophysical properties, such as porosity and density, and mineralogy (see e.g. Clauser 2006; Fuchs et al. 2013; Pauselli et al. 2021 and references therein). An extensive overview of different models can be found in Abdulagatova et al. (2009). Commonly, these models are classified into mixing models, which are solely based on geometrical considerations, and empirical models. The arithmetic, harmonic and geometric means are the most widely used models among the theoretical models. These models use thermal conductivity values of the individual rock components and their corresponding volume fractions as input parameters. They differ in the assumption of the spatial distribution of the solid components and the pore space, including the pore fluid. The arithmetic mean assumes components arranged in parallel, with heat flow aligned parallel to them. In contrast, the harmonic mean assumes heat flow perpendicular to the arrangement, whereas the geometric mean model assumes a random distribution of components without a preferential alignment. Some theoretical models include an additional uncertainty factor related to pore and particle structure expressed by an empirically derived constant. For example, De Vries (1963) developed a semi-empirical model for unconsolidated materials based on the Maxwell equation, which includes a shape factor g for oblate ellipsoids of rotation. Pichugin et al. (2022) reviewed several studies that derive correction factors for the geometric mean model. Thus, they obtained average correction factors f for different rock types and pore fluids. Sugawara and Yoshizawa (1961) empirically derived an equation for estimating bulk thermal conductivity from controlled laboratory measurements using materials with defined geometry. Finally, they introduced an empirical constant n that depends on pore geometry and tested it on sandstones.

Further studies focused on developing empirical models for site-specific sandstones (e.g. El Sayed 2011; Nabawy and Géraud 2016). From laboratory analyses of specific sandstones, linear or log-linear relationships between thermal conductivities and material properties were established by correlating petrophysical properties, such as porosity and density, and mineral contents with measured thermal conductivities. For example, El Sayed (2011) evaluated 35 samples of non-homogeneous, fine-grained sandstones from the Bahariya formation (Egypt) to develop an empirical model based on porosity, bulk density and permeability. Nabawy and Géraud (2016) evaluated 19 samples of the Nubia sandstones (Egypt), which are characterised by high porosities (~ 25–39%), to build an empirical model based on the mineral content (clay and quartz) and porosity.

The ability of mathematical models to accurately estimate thermal conductivities is usually evaluated by comparing the estimated values against laboratory measurements. However, estimated thermal conductivities have yet to be compared against field measurements from depth-resolved TRT. Menberg et al. (2013) compared estimated thermal conductivities from mathematical models (i.e. arithmetic, harmonic and geometric mean; De Vries 1963) against depth-averaged effective thermal conductivity determined with a conventional TRT. The best fit for the analysed unconsolidated sediments was obtained with the geometric mean model.

This study focuses on analysing the thermal conductivity of Triassic Buntsandstein sandstones. We identify theoretical models that can be used to determine the thermal conductivity of the sandstones and yield comparable results to laboratory and field tests. First, the material properties, mineralogy and thermal conductivity of core samples from Triassic sandstones were measured in the laboratory. Known theoretical models were then applied to estimate the thermal conductivities of the core samples and verified against laboratory measurements. Finally, the estimated and measured thermal conductivities were compared to depth-resolved, effective thermal conductivities obtained with an ETRT. Thus, challenges in comparing laboratory and in-situ thermal conductivities are identified and discussed.

Study site and geological background

The study site is located in Neuweiler in the northern Black Forest, Germany (Fig. 1a), where a borehole with a borehole radius of 0.089 m was drilled in sedimentary rocks of the Lower Triassic. Stratigraphically, the rocks likely span from the Olenekium (251–247.5 million years) to the Anisium (247.5–241 million years). They were encountered in the locally mappable formation of the Upper to Middle Buntsandstein (Fig. 1c). From 0 to 35.3 m bgl, the "Plattensandstein" formation (Anisium) was encountered, including two weathering horizons between 11.5 and 19.2 m bgl, and one paleosol between 23.4 and 25.6 m bgl. At 35.4–39.1 m bgl, another weathering horizon marks the transition zone to the underlying "Kristallsandstein" sub-formation (Olenekium). The "Kristallsandstein" formation extends up to a depth of 50.9 m bgl, where another weathering horizon initiates the "Geröllsandstein" sub-formation (Olenekium), which is encountered up to the final borehole depth. Generally, the upper layers are predominantly characterised by fine sandstones with a high occurrence of mudstones in the first ten meters. From about 42.2 m bgl, alternating strata of fine and medium sandstones are found. The underlying layers are mainly characterised by medium sandstones. These sandstones are

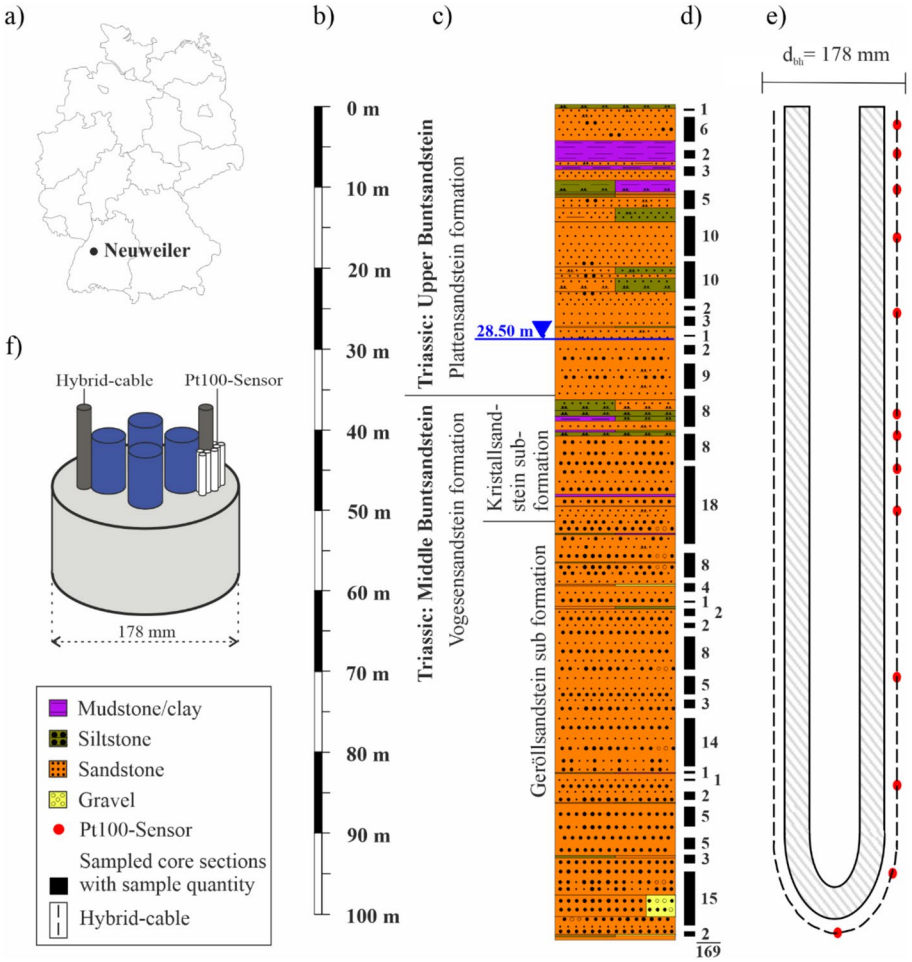

Fig. 1 Overview of the study site in Neuweiler, Germany: **a** location, **b** borehole depth, **c** stratigraphy with geological profile including, **d** number of samples, **e** arrangement of the hybrid cable and temperature probes (Pt100) and **f** schematic setup

strongly silicified within the "Kristallsandstein" formation (Günther 2010). The unconfined groundwater level was measured at a depth of 28.5 m bgl. In total, 169 samples were collected from the drill cores (Fig. 1d), representing homogeneous sections of the borehole profile. Since some samples were in poor condition, laboratory analyses were feasible only on 156 samples.

Methods

The thermal conductivities of the Triassic sandstones were evaluated using several methods. First, the thermal conductivities of the samples were measured in the laboratory (λ_{sat}). In addition, petrophysical, mineralogical and structural properties of the samples, such as porosity and bulk density, were determined. Then, the thermal conductivities (λ_{est}) were estimated with theoretical models and compared with the laboratory measurements. Finally, effective thermal conductivities (λ_{eff}) were determined with an ETRT. The individual methods are described in detail in the following paragraphs.

Laboratory analyses

Thermal conductivity was measured of samples at dry (oven drying at 105 °C) and at saturated conditions. The samples' minimum length was from 50 to 200 mm. They were cut and polished to have three flat sides. To saturate the samples, the dry samples were placed in a desiccator and vacuumed for four hours. Afterwards, the degassed samples were immersed in degassed tap water for at least 12 h to allow for complete saturation.

Thermal conductivity was measured with the transient hot wire method as a half-space line source using surface probes (ISOMET 2104, Applied Precision Ltd., Slovakia; measurement accuracy provided by the manufacturer is 10%). Measurements were repeated four times on each of the three flat sample surfaces, resulting in N = 12 measurements. Measurement uncertainties were calculated according to the Guide to the expression of uncertainty in measurements (ISO IEC 98-3 2008). Considering a 10% accuracy of the measurement device, the standard deviation and student-t-distribution, the measurement uncertainty was between 10 and 11%. Table 1 summarises the determined material properties and the corresponding measurement methods. All measurements were carried out in accordance with the German Institute of Standardisation (DIN). The mineralogy of ten selected samples was determined by modal analysis using a polarisation microscope (AXIO Scope.A1, Carl Zeiss Microscopy GmbH, Germany). The mineral content was quantified by manual point counting.

Table 1 Petrophysical, mineralogical and structural analysis methods used on the Triassic sandstone samples

	Parameter	Method	Measurement uncertainty
Petrophysical analysis	Water content w	Oven drying (DIN EN ISO 17892–1, Deutsche Norm 2015)	±0.002 g accuracy of the scale and 1% handling error, $N = 1$
	Bulk densities ρ_d, ρ_b	Immersion weighing (DIN EN 1936, Deutsche Norm 2007)	±0.002 g accuracy of the scale and 1% handling error, $N = 1$
	Solid density ρ_s	Capillary pycnometer (DIN EN 1936, Deutsche Norm 2007)	±0.0005 g accuracy of the scale and 1% handling error, $N = 2$
	Permeability K	TinyPerm 3	Standard deviation from 10 measurements at different positions on the 1–6 sample surfaces ($N = 20$–60)
Mineralogical analysis	Carbonate content CO_3	Gasometric determination (DIN 18129, Deutsche Norm 2011)	±0.0005 g accuracy of the scale, ±0.1 mL accuracy of gas volume, $N = 2$–4
	Mineral components (quantitative)	Polarisation microscopy	Assuming a 10% error, $N = 2$
Structural analysis	Average pore diameter d_{pore} Average inner pore surface A_{pore}	Mercury porosimetry (DIN ISO 15901–1, Deutsche Norm 2019)	Assuming a 15% error (based on the deviation between matrix densities from MIP and solid density), $N = 1$
	Texture Grain size Grain contacts Degree of sorting and roundness Porosity and pore filling	Polarisation microscopy	

N = number of measurements

The water content was analysed for the re-saturated samples. Based on the results of the laboratory measurements, the open porosity ϕ_{open} was determined from the evaporable water content w at saturated conditions as follows (DIN EN 1936, Deutsche Norm 2007):

$$\phi_{open} = \frac{w\rho_d}{\rho_w} \tag{1}$$

with ρ_d being the dry bulk density and ρ_w being the density of water at a defined temperature. Moreover, total porosity ϕ was determined from the solid density ρ_s by applying the following equation:

$$\phi = 1 - \left(\frac{\rho_d}{\rho_s}\right) \tag{2}$$

Theoretical estimation of thermal conductivity

The theoretical models used to estimate thermal conductivity are summarised in Table 2. They are commonly used in literature and require a limited number of material properties.

The mixing models assume fully water-saturated samples, with the thermal conductivity of the pore fluid (λ_f) equal to that of water ($\lambda_w = 0.598$ W m^{-1} K^{-1} at T = 20 °C). The thermal conductivity of the solid matrix λ_s was calculated with the geometric mean using the thermal conductivities of the minerals λ_i provided in Table 3. The thermal conductivity of the lithic fragments was calculated estimating a composition of 80% quartzite, 15% mica and 5% claystone from polarisation microscopy. The mineral composition was analysed in only ten samples representing homogeneous lithological zones. The average matrix thermal conductivity of these ten samples was then adopted for the model evaluation of the remaining 131 samples.

The semi-empirical models were evaluated by assuming empirical parameters using the information available from the different studies. For the De Vries (1963) model, the shape factors $g_i = \{0.75, 0.125, 0.125\}$ are applied (De Vries 1963; Woodside and Messmer 1961). In accordance with Pichugin et al. (2022), the correction factor $f = 0.65$ was applied to the weighted geometric mean model, assuming monomictic and saturated sandstones. Sugawara and Yoshizawa (1961, 1962) derived two empirical constants n for their model, which correspond to two different sets of sandstones, $n = 2.5$ and $n = 2$, and were both adopted in this study.

Two empirical models developed for different sandstones were evaluated. To apply the model by El Sayed (2011), porosity, bulk density and permeability were determined according to the methods described in Table 1. Since the model by Nabawy and Géraud (2016) is based on quartz and clay content, the model was only applied to the ten samples with evaluated mineralogy.

Field measurements

A double U-pipe BHE with an outer pipe diameter of 0.032 m was installed in the borehole, which was grouted afterwards with a backfill material (Füllbinder H-hs PLUS, Schwenk Zement GbH &Co. KG, $\lambda_{grout} \geq 1.0$ W m^{-1} K^{-1}). The BHE is equipped

Table 2 Theoretical models to estimate thermal conductivities

Type	Model name	Equation		Assumptions and reference
Mixing models	Arithmetic mean	$\lambda_{ari} = \phi\lambda_f + (1-\phi)\lambda_s$	(3)	Theoretical maximum, heat flow parallel to a layered material
	Harmonic mean	$\frac{1}{\lambda_{har}} = \frac{\phi}{\lambda_f} + \frac{1-\phi}{\lambda_s}$	(4)	Theoretical minimum, heat flow perpendicular to a layered material
	Geometric mean	$\lambda_{geo} = \lambda_f^{\phi}\lambda_s^{(1-\phi)}$	(5)	Mean constrained within the bounds of the theoretical minimum and maximum
	Voigt-Reuss-Hill average	$\lambda_{VRH} = 0.5(\lambda_{arit} + \lambda_{har})$	(6)	Mean of theoretical maximum and minimum, Hill (1952)
	Statistical spatial distribution mean	$\lambda_{SSD} = \sqrt{\lambda_{ari}\lambda_{har}}$	(7)	Assuming a layered arrangement of mineral components, Pribnow and Umsonst (1993)
	Hashin–Shtrikman upper bound	$\lambda_u = \lambda_s + \phi\left(\frac{1}{\lambda_f-\lambda_s} + \frac{1-\phi}{3\lambda_s}\right)^{-1}$	(8)	Narrower bounds, derived for effective elastic moduli of a multiphase material of arbitrary phase geometry, Hashin and Shtrikman (1963)
	Hashin–Shtrikman lower bound	$\lambda_l = \lambda_f + (1-\phi)\left(\frac{1}{\lambda_s-\lambda_f} + \frac{\phi}{3\lambda_f}\right)^{-1}$	(9)	
	Hashin–Shtrikman average	$\lambda_{ave} = 0.5(\lambda_u + \lambda_l)$	(10)	
(Semi-)empirical, considering pore geometry	de Vries	$\lambda_{Vries} = \frac{\phi\lambda_f + (1-\phi)F_1\lambda_s}{\phi + (1-\phi)F_1}$ $F_1 = \frac{1}{3}\sum_{i=1}^{3}\left[1 + \left(\frac{\lambda_s}{\lambda_f} - 1\right)g_i\right]^{-1}$	(11)	Based on the Maxwell-Eucken equation, including a geometrical shape factor g_i of the solid particles, De Vries (1963)
	Weighted geometric mean	$\lambda_{est} = \lambda_f^{f\phi}\lambda_s^{(1-f\phi)}$	(12)	Based on the geometric mean, including a rock-specific empirical *f*-constant, Pichugin et al. (2022)
	Sugawara and Yoshizawa	$\lambda_{est} = (1-A)\lambda_s + A\lambda_f$ $A = \left[\frac{2^n}{2^n-1}\right]\left\{1 - \left[1/(1+\phi)^n\right]\right\}$	(13)	Empirically derived model, including a rock-specific empirical *n*-constant, Sugawara and Yoshizawa (1961)
Empirical	El Sayed	$\lambda_{est} = 3.003 + 0.533\phi + 0.044\rho_b - 0.091logK$	(14)	Derived from 35 samples, El Sayed (2011)
	Nabawy and Géraud	$\lambda_{est} = 0.022Qz - 0.0456Cl - 0.069\phi_W + 3.18$	(15)	Derived from 19 samples, Nabawy and Géraud (2016)

Thermal conductivity of the pore fluid (λ_f), thermal conductivity of the solid matrix (λ_s), quartz content (*Qz*), clay content (*Cl*), porosity (φ), porosity measured with water injection (φ_w), permeability (*K*), bulk density (ρ_b)

with a hybrid cable, four optic fibres for temperature measurements and four copper conductors as heating elements (Helukom® A-DSQ(ZN)B2Y, 1 × 4 G 50/125 + Cu 4 × 1.5 mm^2, length = 234 m), at the outside of one U-pipe (experimental setup see Fig. 1e, f). The ETRT is conducted over the duration of about 186 h by applying an average specific heat load of 32 W m^{-1} (PowerTen Power Ten Inc. R66E-60220 DC

Table 3 Thermal conductivity values of the mineral components used for the calculation of matrix thermal conductivities based on Schön (2011) and their estimated weighing factors

Mineral	Thermal conductivity λ_i [W m^{-1} K^{-1}]	Weighing factor [-]
Quartz	7.7	mineral content from polarisation microscopy
Feldspar (Microcline)	2.5	mineral content from polarisation microscopy
Lithic fragments, including:		mineral content from polarisation microscopy
Quartzite	5.1	0.8
Mica [a]	2.3	0.15
Claystone	2.0	0.05

[a] value for muscovite

Power Supply, data logger ALMEMO 2590, AHLBORN). The specific heat load was determined from voltage (accuracy ± 0.1% of the full-scale value of 200 V + 2 digits + 0.03% of the measurement value + 2 digits) and current (accuracy ± 0.1% of the full-scale value of 200 mV + 2 digits + 0.03% of the measurement value + 2 digits + 0.5% uncertainty of the shunt). The temperature was measured at 60 s intervals using DTS with a measurement interval of 1 m (Agilent, AP Sensing, N4386B, dual-ended measurement, measurement uncertainty provided by the manufacturer is ± 0.2 K).

As the hybrid cable was installed in a loop, the temperature data of two corresponding length intervals of the optic fibre were averaged for each depth interval. The effective thermal conductivity (λ_{eff}) was evaluated using the infinite line source (ILS) model as given in Eqs. 16 and 17 (Carslaw and Jaeger 1959; Gehlin 2002):

$$T(r,t) - T_0 \approx \frac{q}{4\pi\,\lambda_{eff}}\left(\ln\left(\frac{4\alpha t}{r_b^2}\right) - \gamma\right) + qR_{th} \tag{16}$$

$$\lambda_{eff} = \frac{q}{4\pi m}; m = \frac{\Delta T}{\Delta \ln(t)} \tag{17}$$

$T(r,t)$ is the temperature at a defined distance r from the heat source and a specific time t. T_0 is the undisturbed subsurface temperature at time $t = 0$, and α is the thermal diffusivity calculated as:

$$\alpha = \frac{\lambda_{eff}}{\rho c_p} \tag{18}$$

assuming a volumetric heat capacity of the subsurface ρc_p of 2.3 MJ m^{-3} K^{-1} (Verein Deutscher Ingenieure 2010). r_b is the borehole radius, R_{th} is the thermal borehole resistance, γ is Euler's constant and m is the slope of the linear regression line. The starting evaluation time is defined by applying the theoretical criterion:

$$t_{start} = \frac{Pr_b^2}{\alpha} \tag{19}$$

where P = 10 (Gehlin 2002). In accordance with the German technical guideline VDI 4640-5 (Verein Deutscher Ingenieure 2020), thermal conductivity was evaluated with the sequential forward evaluation by iteratively increasing the number of the evaluated

datapoints. The resulting thermal conductivities were checked for independence of the test time by applying the convergence criterion $\Delta\lambda_{eff}/\lambda_{eff}<0.05/20$ h. The uncertainty of the effective thermal conductivity from ETRT was calculated based on Witte (2013) from the uncertainty of the specific heat load and standard uncertainty of the slope, adding a 5% model error, and was about 9%.

Results and discussion

Laboratory results

The laboratory results are summarised in Fig. 2. A table including the values is also provided in the supporting information (Supplementary results, Table A-1).

The results indicate a large variability of thermal properties of the Triassic sandstones (Fig. 2a), as also reported in literature (Franz and Schulze 2016; Kämmlein and Stollhofen 2019a). The average thermal conductivity of saturated core samples is 4.6 W m^{-1} K^{-1} with values ranging between 2.7 ± 0.28 and 6.4 ± 0.6 W m^{-1} K^{-1}.

Porosities range between 5.6 ± 0.1 and 23.6 ± 0.4% (Fig. 2b). They are very strongly negatively correlated with the dry bulk densities (Pearson correlation coefficient r = 0.96), as higher bulk densities are related to a denser packaging of the particles. The assessment of the pore geometry shows average pore diameters ranging between 0.010 ± 0.001 and 1.04 ± 0.16 µm with an average value of 0.14 µm (Fig. 2e). The average inner pore

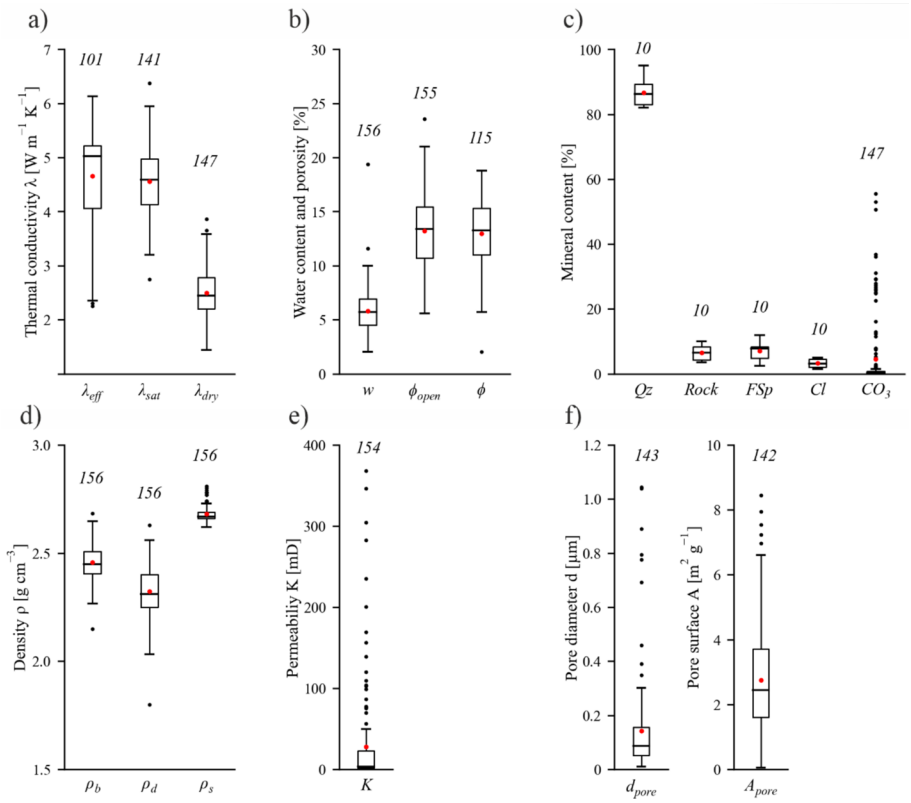

Fig. 2 Petrophysical properties of the Triassic sandstones. Number of samples in italics and mean values in red: **a** thermal conductivities, **b** water content and porosities, **c** mineral contents, **d** densities, **e** permeability, **f** pore diameter and inner pore surface from mercury intrusion porosimetry

surface is 2.75 $m^2\ g^{-1}$ covering a wide range of values from 0.06 ± 0.01 to $8.5 \pm 1.3\ m^2\ g^{-1}$ (Fig. 2f). The correlation with the laboratory-derived thermal conductivity of saturated samples indicates decreasing thermal conductivities with increasing inner pore surface ($r = 0.63$).

The mineral contents of the ten representative samples vary only slightly (Fig. 2b). The samples predominantly consist of quartz (82 ± 8–$95 \pm 10\%$), feldspar (especially microcline, 3 ± 1–$12 \pm 6\%$), clay (1.5 ± 0.9–$5.0 \pm 0.5\%$), carbonate ($0.06 \pm 0.03\%$–55 ± 5) and lithic fragments ($4 \pm 1\%$–$10 \pm 1\%$). Hematite was found with contents < 1%. As quartz has a high thermal conductivity (7.7 $W\ m^{-1}\ K^{-1}$ in Schön, 2011), higher quartz contents result in higher matrix thermal conductivities and, therefore, in higher bulk thermal conductivities. A correlation coefficient of $r = 0.80$ (10 samples) is determined between quartz content and saturated thermal conductivities. The repeated analysis of the mineral content shows a high uncertainty due to the heterogeneous distribution of the minerals in the optically homogeneous impression of the sample.

The permeability of the Triassic sandstones (Fig. 2d) shows a large variation with values ranging between 1.2 ± 1.4 and 368 ± 213 mD and a mean value of 28.0 mD. The high measurement uncertainties result from the measurements at different positions on the sample surfaces. A corresponding median of 3.2 ± 2.7 mD indicates a strong skewness in the distribution towards low permeabilities.

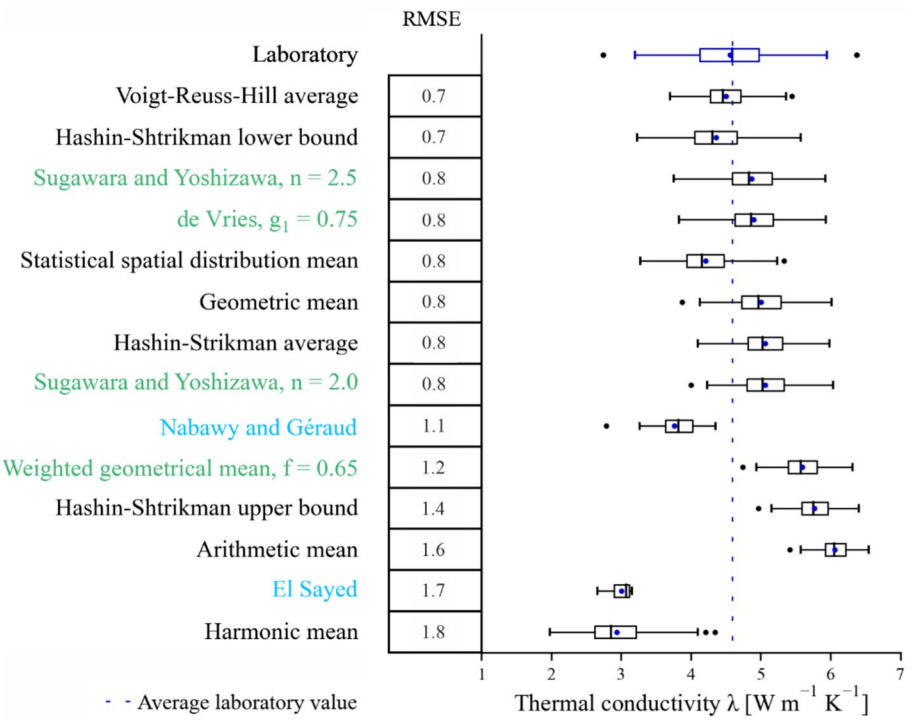

Fig. 3 Thermal conductivities derived using various mathematical models sorted according to the root mean square error (RMSE). The models are classified into theoretical (black), semi-empirical (green) and empirical models (blue)

Estimated thermal conductivity

The estimated thermal conductivities from the different theoretical models are illustrated in Fig. 3 and summarised in the supporting information (Supplementary results, Table A-2). The model performance is evaluated by comparing the estimated thermal conductivities and the laboratory results.

The average root mean square error (RMSE) of all applied models is 1.0 W m^{-1} K^{-1}. The best agreement is achieved with the Voigt-Reuss-Hill model with an average estimated thermal conductivity of 4.6 W m^{-1} K^{-1} and an RMSE of 0.7 W m^{-1} K^{-1}, which corresponds to 15% of the mean thermal conductivity measured on the samples. However, several models have acceptable RMSE $\leq$ 0.8 W m^{-1} K^{-1}, which accounts for $\leq$ 18% of the average thermal conductivity (Fig. 3). Among them are the statistical spatial distribution mean, the model by Sugawara and Yoshizawa, the de Vries model, the geometric mean model and the Hashin–Shtrikman average.

Mixing models

Figure 3 shows that models assuming randomly distributed components (geometric mean, Voigt-Reuss-Hill average, statistical spatial distribution mean, average Hashin–Shtrikman mean) are in good agreement with the average thermal conductivity of the Triassic sandstone samples at saturated conditions. Porosity is an important influencing parameter in all theoretical models. However, the porosity value only provides one bulk value of the percentage of the pore space, and does not take into account the topology (connectivity), the geometry of the pores and the inhomogeneity of the pore space. Yet, the characteristics of the pore space were shown to influence heat conduction (e.g.

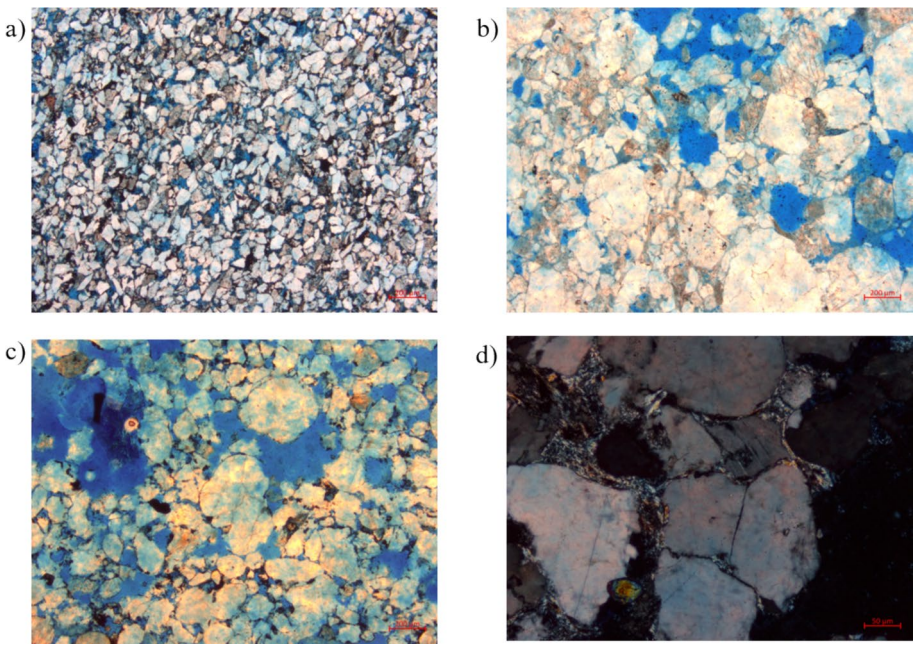

Fig. 4 Exemplary polarisation microscopy images from thin sections, **a** arrangement of particles (bright field, sample at 58.1 m), **b** inhomogeneity of pore size (bright field, sample at 100.1 m), **c** varying degrees of roundness (bright field, sample at 61.2 m), **d** varying pore filling (crossed polarisers, sample at 95.6 m)

Albert et al. 2017; Midttomme and Roaldset 1998). To further investigate this influence for the ten selected samples, polarisation microscopy was used to qualitatively assess pore geometry and the matrix distribution (Fig. 4).

Figure 4a exemplary shows the arrangement of silt particles building the rock matrix. Most samples showed an irregular distribution of the pore space and local accumulation of smaller or larger grains (Fig. 4b). The degree of roundness, as well as the number and kind of grain contacts vary widely (Fig. 4c, d). In theory, more contacts and a higher contact surface result in higher thermal conductivities. Hence, in addition to absolute porosity values, material properties such as grain size, pore size and particle contact area are expected to be relevant input parameters for theoretical models. However, quantifying such relationships using qualitative data from thin section analysis is challenging due to the heterogeneity of the microstructure.

Previous studies also tried to quantify the effect of pore connectivity on thermal conductivity. For example, a stronger effect of the pore shape on the thermal conductivity was shown for samples with generally higher porosities (Ordonez-Miranda and Alvarado-Gil 2012). Moreover, Shen et al. (2021) tried to define pore connectivity through the ratio of effective porosity (determined with mercury intrusion porosimetry) and total porosity. They proposed a new model to estimate thermal conductivities based on this relationship that could improve their estimation results (mean deviation < 10% for saturated samples). These models could potentially estimate thermal conductivities more accurately, but require further laboratory measurements, such as mercury intrusion porosimetry, polarisation microscopy etc.

Semi-empirical models

The semi-empirical models intend to overcome the lack of knowledge on pore geometry by deriving empirical parameters. By applying fitting parameters reported in different studies (De Vries 1963; Pichugin et al. 2022; Sugawara and Yoshizawa 1962, 1961), thermal conductivities were estimated with varying success (Fig. 3). The De Vries (1963) model results in acceptable estimates with an RMSE of 0.8 W m^{-1} K^{-1}, although thermal conductivities are generally overestimated.

The correction of the geometric mean as suggested by Pichugin et al. (2022) gives a worse fit than the original geometric mean model (RMSE of 1.2 W m^{-1} K^{-1} compared to 0.9 W m^{-1} K^{-1}). Pichugin et al. (2022) aim at compensating an underestimation of thermal conductivities with the geometric mean model by setting a fitting parameter of $f < 1$. However, the results of this study show a minor overestimation of thermal conductivities (with an estimated average of 5.0 W m^{-1} K^{-1}), indicating that a fitting parameter $f > 1$ would improve the estimation.

The model of Sugawara and Yoshizawa (1961, 1962) is here applied with two different fitting parameters, derived for two different sets of sandstones. Using a fitting parameter of $n = 2.5$, the average thermal conductivity of 4.9 W m^{-1} K^{-1} is closer to the laboratory-derived thermal conductivity than using $n = 2.0$, which leads to 5.1 W m^{-1} K^{-1}. However, the RMSE is 0.8 W m^{-1} K^{-1} for both fitting parameters.

Empirical models

The two selected empirical models assume linear or log-linear relationships between material properties and thermal conductivities. Both show a large error for the estimated thermal conductivities (Fig. 3). The model by El Sayed (2011) significantly underestimates the thermal conductivities with an average value of 3.0 W m^{-1} K^{-1} and an RMSE of 1.7 W m^{-1} K^{-1}. This model is based on porosity and dry bulk density, and therefore on two significantly inter-correlated properties ("Laboratory results"). Furthermore, the model is based on the decadic logarithm of permeability, which only weakly correlates with thermal conductivity ($r = 0.43$). Accordingly, the permeability does not significantly impact the thermal conductivities of the Triassic sandstones evaluated in this study. As thermal conductivity describes the ability of a material to conduct heat, and permeability describes the ability of a material to transport fluids, both properties define the heat transport properties of a medium. However, they have no clear physical relationship, even if both can be interconnected by porosity.

The model by Nabawy and Géraud (2016) also underestimates the thermal conductivities with an average value of 3.8 W m^{-1} K^{-1}. As this model considers the quartz and clay content, it was only applied to the ten samples with quantified mineralogy, which reduces the statistical significance of the results. Moreover, in the selected samples, clay does not occur in the form of distinct particles but rather in the matrix, which increases the uncertainty of the mineral content.

In addition to the aforementioned limitations for applying the empirical models to the samples of this study, our findings also suggest that empirical models derived for a specific set of sandstone samples, cannot be easily transferred to other study sites or other sandstones. Due to differences in sedimentation and consolidation processes, the composition and properties of sandstones are very diverse, which hinders the transferability of empirically derived constants and relationships. In contrast, models based on theoretical considerations, for example, of spatial particle distribution, can be applied to different sandstones or different study sites to estimate thermal conductivities at a laboratory scale within an uncertainty range of 15–20% (Fig. 3).

The limited number of samples analysed with respect to mineralogy is one major limitation for comparing modelled thermal conductivities in this study. The estimated thermal conductivities were calculated with an average matrix thermal conductivity when applying the mixing models and semi-empirical models. The average matrix thermal conductivity was determined based on the mineral content analysed for ten representative samples. The average matrix thermal conductivity is 6.9 W m^{-1} K^{-1} with values ranging between 6.5 ± 1.4 and 7.3 ± 1.4 W m^{-1} K^{-1}. Hence, the range in matrix thermal conductivities is smaller than the uncertainty in their determination. Estimated thermal conductivities calculated with an average matrix thermal conductivity are compared with those calculated from sample-specific matrix thermal conductivities in the Supporting information (Fig. A-1 and Table A-3). This comparison demonstrates that the simplified assumption on the mineralogy does not affect the conclusions drawn from modelled thermal conductivities.

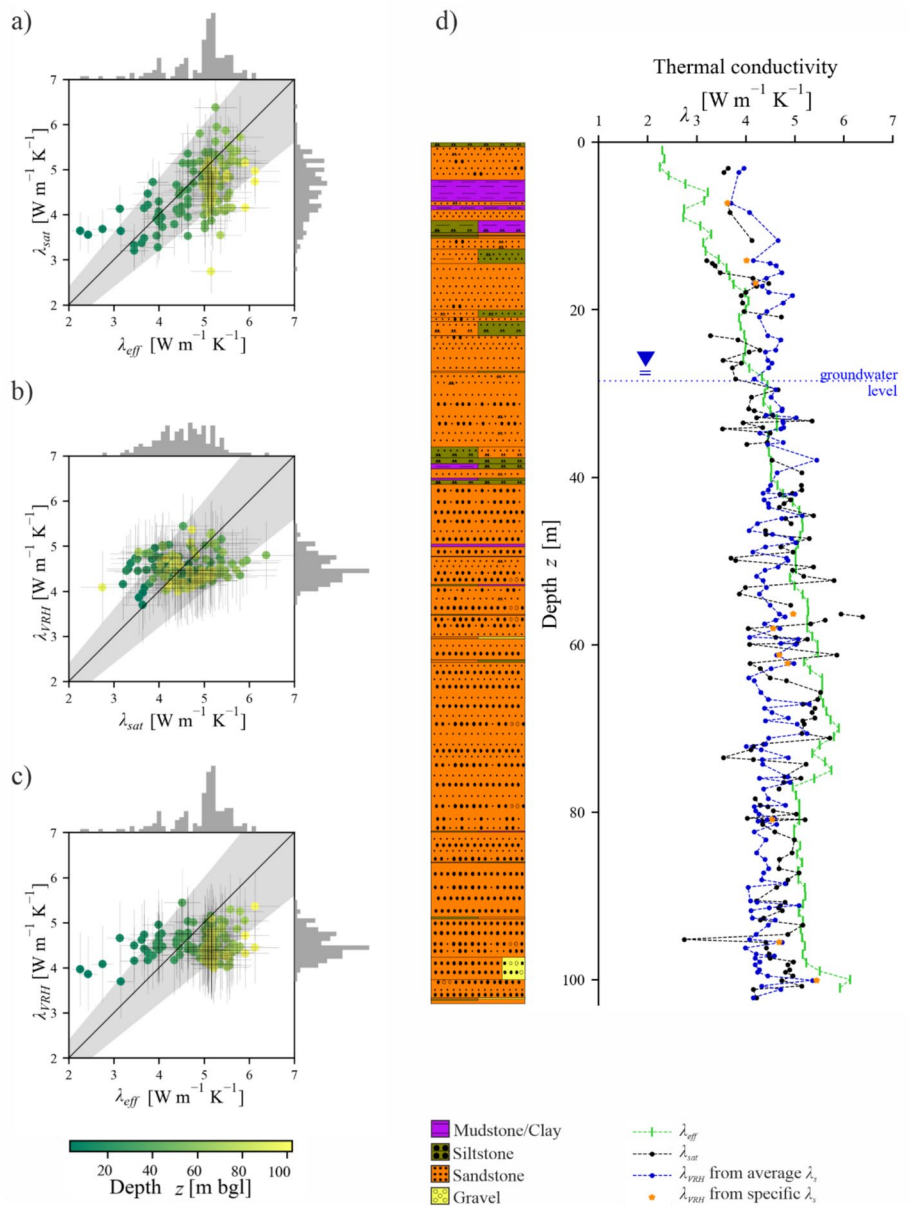

Fig. 5 Comparison of the different methods to determine the thermal conductivities: **a** laboratory (λ_{sat}) and field values (λ_{eff}), **b** laboratory and estimated thermal conductivities applying the Voigt-Reuss-Hill average (λ_{VRH}), **c** estimated (λ_{VRH}) and field values (the grey area indicates an error of 20%, the grey lines indicate measurement uncertainties), **d** depth-specific results

Field results

The estimated thermal conductivities were compared to effective thermal conductivities measured in the field (Fig. 5). The average effective thermal conductivity evaluated with the ETRT was 4.7 W m^{-1} K^{-1} with values ranging between 2.3 ± 0.2 and 6.1 ± 0.4 W m^{-1} K^{-1} (Fig. 2a). Effective thermal conductivities are compared with laboratory values by individually attributing each laboratory value to the corresponding fibre optic depth interval. The difference in the average values between the effective thermal conductivities and the laboratory measurements is only 0.1 W m^{-1} K^{-1}. In Fig. 5a,

the laboratory-derived thermal conductivities are plotted against the effective thermal conductivities.

Both, field and laboratory methods, result in similar value ranges with an RMSE of 0.7 W m^{-1} K^{-1}. Only a few samples have an error > 20% (Fig. 5a). The frequency distribution of the values is complementary shown as marginal distribution. The marginal distribution of the laboratory values is narrower than the field values, which can also be expressed by a lower standard deviation (0.6 W m^{-1} K^{-1}) than that of the ETRT data (0.9 W m^{-1} K^{-1}). This can partly be explained by the differing conditions in the laboratory compared to the field (defined measurement temperature, defined evaluated sample material, solely heat conduction). However, the results also indicate that the laboratory measurements are representative for the effective thermal conductivities of the study site (Fig. 5a).

The marginal distribution of the estimated values using the Voigt-Reuss-Hill model (λ_{VRH}) is significantly narrower than the measured values (Fig. 5b, c), and the standard deviation of the estimated thermal conductivities is comparably low, with 0.3 W m^{-1} K^{-1}. About 18% of the samples show an error > 20%. Potential explanations are linked to the assumptions of the Voigt-Reuss-Hill model. The matrix thermal conductivities of the samples are expressed by an average value of ten representative samples ("Theoretical estimation of thermal conductivity"). Thus, thermal conductivities are mainly dependent on the porosity of the samples. Hence, other possible influencing parameters or conditions are neglected. Plotting the estimated thermal conductivities only for the ten samples with known matrix thermal conductivities reveals that the uncertainty of the assumption is smaller than the observed variability in thermal conductivity (Fig. 5d).

Moreover, Fig. 5c suggests a relation between the thermal conductivities and the borehole depth which cannot be clearly observed in (Fig. 5b). In the deepest section of the borehole, the effective thermal conductivities differ highly from the laboratory-derived values. This can be related to the fact that towards the bottom of the borehole, the assumption of an infinite line source is flawed. Here, heat can propagate not only horizontally but also in vertical (i.e. downward) direction. This results in an overestimation of the effective thermal conductivity. Moreover, larger deviations near the surface of the BHE can be explained by high temperature differences within the first meters of the fibre optic cable and due to surface effects (e.g. Galgaro et al. 2018).

Above the groundwater table, thermal conductivities are overestimated with the laboratory measurements and the Voigt-Reuss-Hill model (Fig. 5d). This can be explained by different water saturations in-situ compared to laboratory measurements and the conditions assumed in the theoretical models. Laboratory measurements are conducted on fully water-saturated samples, and for the theoretical models also full saturation of the pore space is assumed. In theory, partial saturation could be considered in the mathematical models. However, measuring the in-situ water saturation of core rock samples is experimentally challenging (Dalla Santa et al. 2022). By using the laboratory-derived thermal conductivities of dry and saturated samples, a range can be defined for the thermal conductivity of partially saturated samples.

Below the groundwater table (> 28.5 m bgl), especially at depths > 60 m, the effective thermal conductivities tend to be higher than laboratory-derived thermal conductivities (Fig. 5d). This is likely related to groundwater flow which can enhance the

effective thermal conductivities in the field. Previous studies showed that groundwater flow can also impede evaluation of the TRT as results obtained from the ILS approach show an increased sensitivity to the chosen evaluation time step (see e.g. Albers et al. 2024; Angelotti et al. 2018; Katsura et al. 2006; Sanner et al. 2005; Verdoya et al. 2018). However, in this study, a valid evaluation with the ILS is obtained with effective thermal conductivities converging towards a stable value for all depths below the groundwater level. Hence, the higher values cannot clearly be attributed to groundwater flow. Furthermore, it should be noted that the estimation of effective thermal conductivities from laboratory measurements is limited to study sites with negligible groundwater flow velocities as advective heat transport can significantly increase the effective thermal conductivities determined with an ETRT (Albers et al. 2024; Dalla Santa et al. 2022; Luo et al. 2015).

Figure 5a, c show a cluster of effective thermal conductivities at around 5.1 W m^{-1} K^{-1}, which is not reflected in laboratory-measured and estimated thermal conductivities. An explanation for this observation can be found in the measurement principles and the varying sample sizes. Laboratory measurements (and estimation using mathematical models) are point measurements, whereas the ETRT yields average values for 1 m depth intervals. Hence, small-scale changes in lithology, and therefore thermal conductivities, which are represented by thin layers, cannot be properly resolved with the DTS. This also leads to a smoother depth-profile for effective thermal conductivity (Fig. 5d). The comparison between laboratory and field measurements is further limited, as laboratory samples represent the lithology at the borehole, while the ETRT analyses the rock volume outside of the borehole. The sample dimensions are significantly different, with a few centimetres in the laboratory, opposed to a penetration depth of the heat signal of about 1.7 m during the ETRT (as estimated with the ILS model). Especially for sandstones, the properties can be horizontally and vertically heterogeneous due to the variability in the sedimentation conditions and diagenetic processes.

One major limitation of this study is that the anisotropy of thermal conductivity is not considered. Mixing models, such as the Voigt-Reuss-Hill model, assume isotropic properties. Moreover, the surface probe used for thermal conductivity measurement captures a mixed signal from heat flow in all spatial directions, yielding averaged thermal conductivities. By measuring thermal conductivity at three perpendicular sample surfaces, the heterogeneity of the sample is captured, but not the anisotropy in thermal conductivity. In contrast, effective thermal conductivities from ETRT are evaluated assuming radial heat flow. Thus, they represent horizontal thermal conductivities, which may result in higher values due to horizontal layering effects.

The method comparison shows that laboratory-measured as well as estimated thermal conductivities of saturated core samples can represent the effective thermal conductivities of the Triassic sandstones at the study site within an uncertainty of about 15–20%. No model is really satisfying. The “best” model shows an error > 20% for 18% of the analysed samples. The quality of the determined average thermal conductivities for a study site depends on the number of samples. Even though the lithology is dominated by sandstones, the obtained thermal conductivities range between 2.7 ± 0.3 and 6.4 ± 0.6 W m^{-1} K^{-1}. With 156 core samples from one borehole, this study has an

exceptionally high resolution over depth. Another limitation is the high uncertainty in the mineral content, based on the analysis of two aliquots for only ten samples, which impacts the thermal conductivity estimates. Additional mineral analyses could reduce this uncertainty and strengthen the interpretations and comparisons.

The thermal conductivity values are generally within, but slightly higher than the values reported in the literature, which vary between 1.7 and 5.8 W m^{-1} K^{-1} (Franz and Schulze 2016; Haffen et al. 2017; Kämmlein and Stollhofen 2019a). The German industrial guideline VDI 4640, part 1 provides thermal conductivities for sandstones between 1.9 and 4.6 W m^{-1} K^{-1}. Our study shows that, for the Buntsandstein site, the upper bound of this range serves as a good initial estimate.

Conclusion

The aim of this study is the determination of depth-specific thermal conductivities of Triassic Buntsandstein sandstones. Hence, we obtained thermal conductivities from laboratory analyses, theoretical models and ETRT, and compared the various approaches. From this study, we conclude that:

1. Effective thermal conductivities range between 2.3 and 6.1 W m^{-1} K^{-1} with an average of 4.7 W m^{-1} K^{-1}, which makes the Triassic Buntsandstein highly suitable for shallow geothermal systems, such as GSHP systems. The observed heterogeneity highlights the importance of in-situ thermal conductivity determination for shallow geothermal applications.
2. None of the applied theoretical models achieved satisfying results. The Voigt-Reuss-Hill model achieved the best agreement with an RMSE of 0.7 W m^{-1} K^{-1}. Other theoretical models that assume randomly distributed components (e.g. geometric mean, statistical spatial distribution, Hashin–Shtrikman average) estimated thermal conductivities with similar errors. This can partly be explained by the uncertainties in mineral composition and the matrix thermal conductivity determination. Hence, theoretical models only allow for an approximate estimation of thermal conductivities of studied Triassic sandstones.
3. Laboratory measurements and theoretical models achieved only a specific level of accuracy with an RMSE of $\geq$ 0.7 W m^{-1} K^{-1}, when comparing them to effective thermal conductivities from ETRT. The challenges of this comparison are demonstrated, including differences in sampling and measurement principles, limited sample quantity, varying saturation and the possible influence of groundwater flow.

Finally, the findings of this study highlight the importance of choosing an appropriate method for evaluating the thermal conductivities of the Triassic sandstones. Laboratory measurements and theoretical models were less effective compared to in-situ measurements, such as the ETRT. Nevertheless, the comparison of different approaches improved our understanding of the parameters and processes influencing the thermal conductivity of sandstones.

Abbreviations

A_{pore}	Average inner pore surface [m^2 g^{-1}]
bgl	Below ground level

BHE	Borehole heat exchanger
Cl	Clay content [%]
CO_2	Carbon dioxide
CO_3	Carbonate content [%]
d_{pore}	Average pore diameter [µm]
DTRT	Differential thermal response test
DTS	Distributed temperature sensing
E_i	Exponential integral
ETRT	Enhanced thermal response test
f	Rock-specific empirical f-constant [-]
Fsp	Feldspar content [%]
g_i	Geometrical shape factor [-]
ILS	Infinite line source model
K	Permeability [mD]
m	Slope [K ln(s)$^{-1}$]
n	Rock-specific empirical n-constant [-]
q	Specific heat load [W m^{-1}]
Qz	Quartz content [%]
r	Pearson coefficient
RMSE	Root mean square error
r_b	Borehole radius [m]
Rock	Lithic fragment content [%]
R_{th}	Thermal borehole resistance [m K W^{-1}]
SO_2	Sulphur dioxide
T	Temperature [°C]
t	Time [s]
t_{start}	Theoretical starting time criterion [s]
T_0	Reference temperature [°C]
TRT	Thermal response test
UN	United Nations
w	Water content [%]
z	Depth [m]
α	Thermal diffusivity [m^2 s^{-1}]
γ	Euler's constant
λ	Thermal conductivity [W m^{-1} K^{-1}]
λ_{ari}	Thermal conductivity calculated with the arithmetic mean [W m^{-1} K^{-1}]
λ_{ave}	Thermal conductivity calculated with the Hashin–Shtrikman average [W m^{-1} K^{-1}]
λ_{dry}	Laboratory-measured thermal conductivity of a dry sample [W m^{-1} K^{-1}]
λ_{eff}	Effective thermal conductivity [W m^{-1} K^{-1}]
λ_{est}	Estimated thermal conductivity [W m^{-1} K^{-1}]
λ_f	Thermal conductivity of the pore fluid [W m^{-1} K^{-1}]
λ_{geo}	Thermal conductivity calculated with the geometric mean [W m^{-1} K^{-1}]
λ_{grout}	Thermal conductivity of the grouting material [W m^{-1} K^{-1}]
λ_{har}	Thermal conductivity calculated with the harmonic mean [W m^{-1} K^{-1}]
λ_l	Thermal conductivity calculated with the Hashin–Shtrikman lower bound [W m^{-1} K^{-1}]
λ_s	Thermal conductivity of the solid matrix [W m^{-1} K^{-1}]
λ_{sat}	Laboratory-measured thermal conductivity of a saturated sample [W m^{-1} K^{-1}]
λ_{SSD}	Thermal conductivity calculated with the statistical spatial distribution mean [W m^{-1} K^{-1}]
λ_u	Thermal conductivity calculated with the Hashin–Shtrikman upper bound [W m^{-1} K^{-1}]
λ_{VRH}	Thermal conductivity calculated with the Voigt-Reuss-Hill model [W m^{-1} K^{-1}]
λ_{Vries}	Thermal conductivity calculated with the de Vries model [W m^{-1} K^{-1}]
ρ_d	Wet bulk density [g cm^{-3}]
ρ_d	Dry bulk density [g cm^{-3}]
ρ_s	Solid density [g cm^{-3}]
ρ_w	Density of water [g cm^{-3}];
ρc_s	Volumetric heat capacity of the ground [J m^{-3} K^{-1}]
φ	Total porosity [%]
φ_{open}	Open porosity [%

Supplementary Information

The online version contains supplementary material available at https://doi.org/10.1186/s40517-025-00359-0.

Additional file 1

Acknowledgements

The authors would like to thank Dr. PD Kirsten Drüppel, Kristian Nikoloski and Beate Oetzel for their help in preparing, analysing and evaluating the thin sections with polarisation microscopy and XRD analyses. Further, they would like to thank Dr. Petra Huttenloch, Joshua Schnurr and Felix Voss for their help with the laboratory analyses. The helpful comments of the reviewers are also gratefully acknowledged.

Author contributions
A.A., F.G., K.M. and P.B. developed the methodology and designed the study. H.S. and R.Z. acquired the funding. A.A., H.S. and R.Z. carried out the field experiments. H.S., C.F., L.S. and S.W. conducted the laboratory experiments. A.A., F.G. and C.F. executed the data analyses. A.A., F.G. and C.F. created the figures. A.A. and F.G. prepared the draft of the manuscript. All authors read and approved the final manuscript.

Funding
Open Access funding enabled and organized by Projekt DEAL. This study was funded by the funding programmes QEWS II (grant number KIT 03ET1386C, EIFER 03ET1386D) and QEWSplus (grant number KIT 03EE4020D, EIFER 03EE4020E,https://www.qewsplus.de/) by the Federal Ministry for Economic Affairs and Climate Action. The financial support for Kathrin Menberg via the Margarete von Wrangell program of the Ministry of Science, Research and the Arts (MWK) of the State of Baden-Württemberg is gratefully acknowledged.

Data availability
The datasets used and/or analysed during the current study are available from the corresponding author on reasonable request.

Declarations

Ethics approval and consent to participate
Not applicable.

Competing interests
The authors declare no competing interests.**Received: 29 July 2024 Accepted: 2 July 2025**
Published online: 17 July 2025

References

Clauser C. 8 Geothermal Energy. In: Heinloth K. (ed.) Landolt-Börnstein, Group VIII Advanced Materials and Technologies, Volume 3C: (Renewable Energy). Springer-Verlag Berlin Heidelberg. 2006.
ISO IEC 98-3: uncertainty of measurement—Part 3: guide to the expression of uncertainty in measurement GUM: 1995. 2008.
Acuña J, Palm B. A Novel Coaxial Borehole Heat Exchanger: Description and First Distributed Thermal Response Test Measurements. In: Proceedings World Geothermal Congress 2010. Bali, Indonesia. 2010.
Abdulagatova Z, Abdulagatov IM, Emirov VN. Effect of temperature and pressure on the thermal conductivity of sandstone. Int J Rock Mech Min Sci. 2009;46:1055–71. https://doi.org/10.1016/j.ijrmms.2009.04.011.
Abuel-Naga HM, Bergado DT, Bouazza A, Pender MJ. Thermal conductivity of soft Bangkok clay from laboratory and field measurements. Eng Geol. 2009;105:211–9. https://doi.org/10.1016/j.enggeo.2009.02.008.
Albers A, Steger H, Zorn R, Blum P. Evaluating an enhanced thermal response test (ETRT) with high groundwater flow. Geotherm Energy. 2024;12:1. https://doi.org/10.1186/s40517-023-00278-y.
Albert K, Franz C, Koenigsdorff R, Zosseder K. Inverse estimation of rock thermal conductivity based on numerical microscale modeling from sandstone thin sections. Eng Geol. 2017;231:1–8. https://doi.org/10.1016/j.enggeo.2017.10.010.
Angelotti A, Ly F, Zille A. On the applicability of the moving line source theory to thermal response test under groundwater flow: considerations from real case studies. Geothermal Energy. 2018. https://doi.org/10.1186/s40517-018-0098-z.
Bayer P, Saner D, Bolay S, Rybach L, Blum P. Greenhouse gas emission savings of ground source heat pump systems in Europe: a review. Renew Sustain Energy Rev. 2012;16:1256–67. https://doi.org/10.1016/j.rser.2011.09.027.
Blum P, Campillo G, Münch W, Kölbel T. CO2 savings of ground source heat pump systems—a regional analysis. Renewable Energy. 2010;35:122–7. https://doi.org/10.1016/j.renene.2009.03.034.
Carslaw HS, Jaeger JC. Conduction of Heat in Solids. Oxford: Oxford Science Publications; 1959.
Dalla Santa G, Pasquier P, Schenato L, Galgaro A. Repeated ETRTs in a complex stratified geological setting: high-resolution thermal conductivity identification by multiple linear regression. Jgeotech Geoenviron Eng. 2022. https://doi.org/10.1061/(ASCE)GT.1943-5606.0002724.
Deutsche Norm. DIN EN ISO 17892-2, Geotechnische Erkundung und Untersuchung–Laborversuche an Bodenproben–Teil 2: Bestimmung der Dichte des Bodens (ISO 17892-2:2014). 2015.
Deutsche Norm. DIN EN 1936, Natural stone test method Determination of real density and apparent density, and of total and open porosity; German version EN 1936:2006. 2007.
Deutsche Norm. DIN ISO 15901-1, Evaluation of pore size distribution and porosity of solid materials by mercury porosimetry and gas adsorption, Part 1: Mercury porosimetry (ISO 15901-1:2016). 2019.
Deutsche Norm. DIN 18129, Soil, investigation and testing Determination of lime content. 2011.
Franz C, Schulze M. Bestimmung thermischer Eigenschaften der Gesteine des Unteren und Mittleren Buntsandsteins. Grundwasser. 2016;21:47–58. https://doi.org/10.1007/s00767-015-0316-6.
Fuchs S, Schütz F, Förster H-J, Förster A. Evaluation of common mixing models for calculating bulk thermal conductivity of sedimentary rocks: correction charts and new conversion equations. Geothermics. 2013;47:40–52. https://doi.org/10.1016/j.geothermics.2013.02.002.
Gehlin S. Thermal response test: Method Development and evaluation. 2002.
Günther D. Der Schwarzwald und seine Umgebung: geologie, Mineralogie, Bergbau. Stuttgart: Umwelt und Geotourismus. Bornträger Stuttgart; 2010.

Haffen S, Géraud Y, Rosener M, Diraison M. Thermal conductivity and porosity maps for different materials: a combined case study of granite and sandstone. Geothermics. 2017;66:143–50. https://doi.org/10.1016/j.geothermics.2016.12.005.
Hill R. The elastic behaviour of a crystalline aggregate. Proc Phys Soc A. 1952;65:349–54. https://doi.org/10.1088/0370-1298/65/5/307.
Jorand R, Clauser C, Marquart G, Pechnig R. Statistically reliable petrophysical properties of potential reservoir rocks for geothermal energy use and their relation to lithostratigraphy and rock composition: the NE Rhenish Massif and the Lower Rhine Embayment (Germany). Geothermics. 2015;53:413–28. https://doi.org/10.1016/j.geothermics.2014.08.008.
Kämmlein M, Stollhofen H. Pore-fluid-dependent controls of matrix and bulk thermal conductivity of mineralogically heterogeneous sandstones. Geotherm Energy. 2019a. https://doi.org/10.1186/s40517-019-0129-4.
Katsura T, Nagano K, Takeda S, Shimakura K. Heat transfer experiment in the ground with groundwater advection. In: The IEA 10th Energy Conservation Thermal Energy Storage Conference. New Jersey, USA. 2006.
Luo J, Rohn J, Xiang W, Bayer M, Priess A, Wilkmann L, Steger H, Zorn R. Experimental investigation of a borehole field by enhanced geothermal response test and numerical analysis of performance of the borehole heat exchangers. Energy. 2015;84:473–84. https://doi.org/10.1016/j.energy.2015.03.013.
Ma Y, Zhang Y, Cheng Y, Zhang Y, Gao X, Shan K. A case study of field thermal response test and laboratory test cased on distributed optical fiber temperature sensor. Energies. 2022;15:8101. https://doi.org/10.3390/en15218101.
Menberg K, Steger H, Zorn R, Reuß M, Pröll M, Bayer P, Blum P. Bestimmung der Wärmeleitfähigkeit im Untergrund durch Labor- und Feldversuche und anhand theoretischer Modelle. Grundwasser. 2013;18:103–16. https://doi.org/10.1007/s00767-012-0217-x.
Midttomme K, Roaldset E. The effect of grain size on thermal conductivity of quartz sands and silts. Pet Geosci. 1998;4:165–72. https://doi.org/10.1144/petgeo.4.2.165.
Nabawy BS, Géraud Y. Impacts of pore- and petro-fabrics, mineral composition and diagenetic history on the bulk thermal conductivity of sandstones. J Afr Earth Sc. 2016;115:48–62. https://doi.org/10.1016/j.jafrearsci.2015.11.025.
Ordonez-Miranda J, Alvarado-Gil JJ. Effect of the pore shape on the thermal conductivity of porous media. J Mater Sci. 2012;47:6733–40. https://doi.org/10.1007/s10853-012-6616-7.
Pauselli C, Gola G, Ranalli G, Mancinelli P, Trippetta F, Ballirano P, Verdoya M. Thermal conductivity of Triassic evaporites. Geophys J Int. 2021;227:1715–29. https://doi.org/10.1093/gji/ggab293.
Pichugin Z, Chekhonin E, Popov Y, Kalinina M, Bayuk I, Popov E, Spasennykh M, Savelev E, Romushkevich R, Rudakovskaya S. Weighted geometric mean model for determining thermal conductivity of reservoir rocks: current problems with applicability and the model modification. Geothermics. 2022;104: 102456. https://doi.org/10.1016/j.geothermics.2022.102456.
Popov YA, Pribnow DFC, Sass JH, Williams CF, Burkhardt H. Characterization of rock thermal conductivity by high-resolution optical scanning. Geothermics. 1999;28:253–76. https://doi.org/10.1016/S0375-6505(99)00007-3.
Pribnow D, Umsonst T. Estimation of thermal conductivity from the mineral composition: influence of fabric and anisotropy. Geophys Res Lett. 1993;20:2199–202. https://doi.org/10.1029/93GL02135.
El Sayed AMA. Thermophysical study of sandstone reservoir rocks. J Petrol Sci Eng. 2011;76:138–47. https://doi.org/10.1016/j.petrol.2011.01.001.
Shen Y, Wang X, Wang Y, Zhou K, Zhang J, Zhang H, Li J. Thermal conductivity models of sandstone: applicability evaluation and a newly proposed model. Heat Mass Transfer. 2021;57:985–98. https://doi.org/10.1007/s00231-020-02995-7.
Galgaro A, Pasquier P, Schenato L, Cultrera M, Santa GD. Soil thermal conductivity from early TRT logs using an active hybrid optic fibre system. In: IGSHPA Research Track. 2018. p. 1–9.
Spitler JD, Gehlin SEA. Thermal response testing for ground source heat pump systems—an historical review. Renew Sustain Energy Rev. 2015;50:1125–37. https://doi.org/10.1016/j.rser.2015.05.061.
Sugawara A, Yoshizawa Y. An investigation on the thermal conductivity of porous materials and its application to porous rock. Aust J Phys. 1961;14:469–80. https://doi.org/10.1071/PH610469.
Sugawara A, Yoshizawa Y. An Experimental Investigation on the Thermal Conductivity of Consolidated Porous Materials. J Appl Phys. 1962;33:3135–8. https://doi.org/10.1063/1.1728581.
Sanner B, Hellström G, Spitler J, Gehlin S. Thermal Response Test–Current Status and World-Wide Application. In: Proceedings World Geothermal Congress 2005. 2005.
Verdoya M, Pacetti C, Chiozzi P, Invernizzi C. Thermophysical parameters from laboratory measurements and in-situ tests in borehole heat exchangers. Appl Therm Eng. 2018;144:711–20. https://doi.org/10.1016/j.applthermaleng.2018.08.039.
Verein Deutscher Ingenieure: VDI 4640, part 1: thermal use of the underground, Fundamentals, approvals, environmental aspects. 2010.
De Vries DA. Thermal properties of soils. In: Physics of plant environment. North-Holland Publishing Co., Amsterdam. 1963. p. 210–235.
Wilke S, Menberg K, Steger H, Blum P. Advanced thermal response tests: a review. Renew Sustain Energy Rev. 2020;119:109575. https://doi.org/10.1016/j.rser.2019.109575.
Witte HJL. Error analysis of thermal response tests. Appl Energy. 2013;109:302–11. https://doi.org/10.1016/j.apenergy.2012.11.060.
Woodside W, Messmer JH. Thermal Conductivity of Porous Media. I. Unconsolidated Sands. J Appl Phys. 1961;32:1688–99. https://doi.org/10.1063/1.1728419.
Hashin Z, Shtrikman S. A variational approach to the theory of the elastic behaviour of multiphase materials. Journal of the Mechanics and Physics of Solids. 1963.
Schön JH. Physical properties of rocks: a workbook. Elsevier. 2011.
Soyk D. Diagenesis and reservoir quality of the Lower and Middle Buntsandstein (Lower Triassic), SW Germany. 2015.
Verein Deutscher Ingenieure. VDI 4640 part 5, Thermal use of the underground, Thermal response test (TRT). 2020.